JCTC Journal of Chemical Theory and Computation

ARTICLE

pubs.acs.org/JCTC

Excited States and Absorption Spectra of UF_6: A RASPT2 Theoretical Study with Spin−Orbit Coupling

Fan Wei, Guo-Shi Wu, W. H. Eugen Schwarz,† and Jun Li*

Department of Chemistry and Laboratory of Organic Optoelectronics and Molecular Engineering of the Ministry of Education, Tsinghua University, Beijing 100084, China

Supporting Information

ABSTRACT: Uranium hexafluoride (UF_6) is an important compound in nuclear chemistry. The theoretical investigation of its excited states is difficult due to the large number of uranium valence orbitals and ligand lone pairs. We report here a detailed relativistic quantum chemical investigation of its excited states up to about 10 eV using restricted active space second-order perturbation theory (RASPT2). Scalar and spin−orbit (SO) relativistic effects are treated by a relativistic small-core pseudopotential. The RASPT2/SO results remain moderately accurate when the electrons in the active space are restricted to single and double excitations. All eight major spectral peaks corresponding to ligand-to-metal charge transfer have been reproduced within an accuracy of about 0.2 eV and are tentatively assigned. We find that BLYP-based hybrid density functional with 35% Hartree−Fock exchange well reproduce the excitation energies of UF_6.

INTRODUCTION

Uranium hexafluoride (UF_6) is widely used in the uranium enrichment process generating fuel for nuclear reactors and nuclear weapons. Understanding its ground- and excited-state properties is important. Accurate theoretical calculations of molecules containing actinides have been challenging, especially when involving excited states. The difficulties are due to complicated electron correlation effects, to significant scalar relativistic (SR) and spin−orbit coupling (SOC) effects, to the large number of valence and semicore electrons in actinide atoms, and to the complexity of electronic configurations owing to f-electrons. A number of theoretical investigations has been carried out on the ground-state properties of UF_6, including geometries, electronic structures and spectroscopic properties, using ab initio wave function theory (WFT) and density functional theory (DFT).[1−8]

For excited states, WFT electron correlation methods based on the multiconfiguration self-consistent field (MCSCF) approach are often needed. In particular, the complete active space self-consistent field approach with second-order perturbation theory (CASPT2) is commonly used to account for both dynamic and nondynamic electron correlations, respectively.[9,10] CASPT2 with the state functions subsequently interacting through SOC yields reliable transition energies for the low-lying excited states of isolated UO_2^{2+} and $[UO_2Cl_4]^{2-}$.[11] Early multireference configuration interaction calculations with single and double substitutions (MR-CISD) using relativistic effective core potentials (RECP) performed less satisfactory,[12,13] mainly due to the large atomic core chosen for uranium. One may expect that RECP calculations with an appropriate "small core" (i.e., with 60 electrons in the frozen uranium core, 32 electrons in the 5s-5p-5d-6s-6p-5f-6d-7s valence shells being optimized) will perform comparable to all-electron calculations, such as those simulating relativistic scalar and SOC effects by the Douglas−Kroll−Hess (DKH) approximation.[14]

The comparison of theoretically computed electronic spectra with corresponding experimental data helps to calibrate the theoretical methodology and conversely to understand and assign the experimental data. The reported photoabsorption and electron-impact spectra of gaseous UF_6 provide important information about the low-lying excited states.[15,16] Some of these states involve electronic ligand-to-metal charge transfer (LMCT) and have been investigated theoretically.[17−22] Already in 1983, Hay[21] had carried out CIS and CISD calculations on the low-lying excited singlet and triplet states with SOC simulated by a large-core pseudopotential. The excitations correspond to one-electron transitions from the 18 highest occupied orbitals with 36

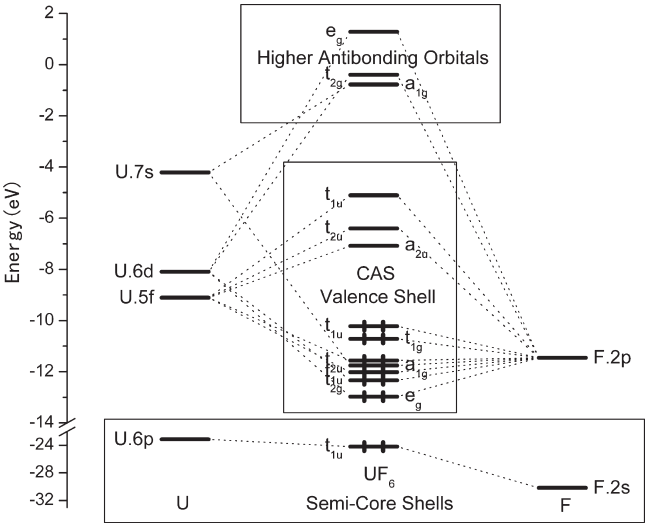

Figure 1. SR Kohn−Sham orbital energy levels of neutral U, F, and UF_6, in eV.[3,22]

Received: January 9, 2011
Published: August 10, 2011

electrons, representing the 6 F^--$2p^6$ shells slightly mixed with U-5f,6p,6d,7s atomic orbitals (AOs), to the 7 lowest virtual ones of U-5f type, see the molecular orbital (MO) level scheme in Figure 1.[21,22] The calculations were quite satisfactory, concerning the low-energy ranges of the experimental spectra. On the other hand, limited by the method, the RECP, the basis sets, and the computer resources of the time, the calculated transition energies of various dipole-allowed $^1T_{1u}$ states were less accurate. In particular, the calculated excitation energies above 7 eV deviated from the experimental ones by as much as 0.8−1.5 eV.

To obtain more accurate results, it is necessary to employ more developed post-HF approaches. In principle, complete active space self-consistent field (CASSCF) with an adequate choice of the active orbitals for the nondynamical correlations, CASPT2 energy improvement for dynamical correlation and subsequent SO-CI for the spin−orbit splittings should produce reliable data. The large near-degenerate valence shell of UF_6 easily leads to configuration spaces of many billions of configuration state functions (CSFs), so that excitation restrictions within the active space become mandatory. The restricted active space (RAS) procedure RASSCF/RASPT2[23] has been successfully applied to CuO_2, Cu_2O_2, and other systems,[24,25] such as UO_2, which shows a similar excitation pattern as UF_6.[26,27]

In the present work we have applied the RASSCF/RASPT2/SO approach to various excited states of the UF_6 molecule. The important SOC effect is accounted for by the common RECP procedure,[28] where the $l\cdot\sigma$ containing one-electron operators[29] also simulate the two-electron spin-coupling effects. After numerous test calculations we have found that RASSCF/RASPT2/SO approach with RASSCF limited to single and double excitations already provides reasonably accurate results for excitations of the F-2p → U-5f type. The experimental excitation energies of UF_6[16] within 10 eV have been well reproduced within about 0.2 eV.

Time-dependent density functional theory (TDDFT) often provides an alternative to account for dynamic electron correlation of excited states.[3,30−32] Previous calculations on actinide complexes indicated that TDDFT excitation energies are of diverse accuracies when comparing with advanced multireference WFT results.[33,34] Therefore a series of TDDFT calculations has been carried out with various exchange−correlation (XC) functionals to further test the reliability of this method for describing the excited states of actinide systems, such as UF_6.

METHODOLOGY AND COMPUTATIONAL DETAILS

All ab initio calculations (HF and post-HF) based on WFT were performed with MOLPRO 2008.[35] The Stuttgart "small core" RECP and the SDD valence basis [12s11p10d8f]/[8s7p6d4f] were used for the U atom,[13] while all-electron aug-cc-pVDZ basis sets were applied for the F atoms.[36] In the present study, we confine ourselves to vertical excitations. The experimental ground-state geometry of UF_6 (O_h symmetry) with an equilibrium bond length of R_{U-F} = 1.999 Å was taken for all states.[37]

In the CASSCF approach, a zeroth-order multireference wave function is generated by a full CI procedure within the CAS specified by (N,M), where N and M are the numbers of correlated electrons and active orbitals. The total number of CSFs rapidly grows with increasing N and M, which virtually limits the applications of CASSCF and CASPT2 to relatively small values of N and M even for present-day computer hardware and software. In the case of UF_6, however, energy and occupation analysis of the MOs, as discussed in the next section, indicates that the effective active space should comprise at least the above-mentioned 36 F^--2p valence electrons and the respective 18 highest occupied and 7 lowest unoccupied orbitals of U-5f type, consistent with the selection of Hay.[21] Such a selection of the minimum active space results in a total of 25 orbitals with 36 electrons, which still excludes the F-2s and U-6s-6p semicore shells and next higher ones of U-6d and -7s type (see Figure 1). A CASSCF calculations using an active space of (36,25) involves nearly 5 billion CSFs (4 940 906 560). However, in an appropriate MO basis, multiple excitations beyond quadruple ones often contribute very little to electron correlation of closed-shell species. Therefore adopting a RASSCF approach, the computational costs can be reduced to a reasonable level.[38]

Table 1. Irreducible Representations of Low-Lying Single-Electron Excited States of UF_6 [a]

orbital transition	excited states	with triplet SOC
$a_1 \rightarrow a_2$	A_2	T_2
$e \rightarrow a_2$	E	T_1, T_2
$a_1 \rightarrow t_1$ or $t_2 \rightarrow a_2$	T_1	A_1, E, T_1, T_2
$a_1 \rightarrow t_2$ or $t_1 \rightarrow a_2$	T_2	A_2, E, T_1, T_2
$e \rightarrow t_1$ or $e \rightarrow t_2$	T_1, T_2	A_1, A_2, 2E, $2T_1$, $2T_2$
$t_1 \rightarrow t_1$ or $t_2 \rightarrow t_2$	A_1, E, T_1, T_2	A_1, A_2, 2E, $4T_1$, $3T_2$
$t_1 \rightarrow t_2$ or $t_2 \rightarrow t_1$	A_2, E, T_1, T_2	A_1, A_2, 2E, $3T_1$, $4T_2$

[a] Without SOC or with singlet SOC, last column with triplet SOC, and the trivial g and u specifications being omitted.

In our RASSCF calculations, the active space of M orbitals is divided into three subspaces, which are referred to as RAS1, RAS2, and RAS3.[35] They contain M_1 doubly occupied MOs, M_2 occupied or partially unoccupied MOs, and M_3 partially or unoccupied MOs, respectively. The total number of CSFs depends also on the chosen level of excitations (n_1,n_3). Index n_1 means that up to n_1 electrons may be excited from the M_1 orbitals of RAS1 into RAS2 or RAS3 and up to n_3 electrons excited from RAS1 or RAS2 into the M_3 orbitals of RAS3. A suitably chosen combination of smaller n_1 and n_3 remarkably decreases the total number of CSFs. Then, a much larger active space of (N,M) can be used in RASSCF than in conventional CASSCF.

The RAS is here defined with reference to the ground-state MO energy level scheme of neutral UF_6 in Figure 1.[3,22] The 18 highest occupied MOs with 36 electrons form RAS1, and the 7 lowest virtual MOs form RAS3, while RAS2 is left empty. Only single and double excitations were included, i.e., $n_1 = n_3 = 2$, since higher excitation levels improve the energy only at the 0.01 eV level. The obtained 1078 CSFs are a fraction of 0.22×10^{-6} of the CSF number of CAS(36,25). Among them, there are 126 excitations of one-electron singlet type and 126 of one-electron triplet type. In this centro-symmetric molecule, half of them are of spatial gerade (g) symmetry, the other half is ungerade (u). The orbital and state symmetry species are listed in Table 1.[39]

Due to parity conservation, the RASSCF/RASPT2 calculations, without or with SOC on top of it, can be performed separately for all g- and u-states. First, state-average single-point RASSCF[40] calculations were carried out to obtain the wave functions for sets of 64 g-singlets (including the ground state) and 63 u-triplets. Then, RASPT2 calculations were performed for each state to improve the dynamic correlation energy. The intruder states problem caused converge troubles for several cases, which were resolved by a common energy-level shift, here by 0.3 au.[41,42]

Table 2. Dominant AO Compositions (in %) and Energies (ε in eV) of the 18 Highest Occupied and 13 Lowest Virtual MOs of the UF_6 Ground State at the DFT-PW91 Scalar and SO Relativistic Levels

scalar relativistic (SR)			SO coupling	
orbital[a]	composition	ε	orbital[b]	ε
	Highest Occupied			
$1e_g$	85 F-2p; 14 U-6d	−12.98	$1u_{3/2g}$	−12.98
$1t_{2g}$	88 F-2p; 12 U-6d	−12.33	$2u_{3/2g}$	−12.36
			$1e_{5/2g}$	−12.29
$1t_{1u}$	79 F-2p; 19 U-5f	−12.02	$1e_{1/2u}$	−12.04
			$1u_{3/2u}$	−12.01
$1a_{1g}$	97 F-2p; 1 U-7s	−11.75	$1e_{1/2g}$	−11.76
$1t_{2u}$	87 F-2p; 13 U-5f	−11.56	$2u_{3/2u}$	−11.56
			$1e_{5/2u}$	−11.55
$1t_{1g}$	100 F-2p	−10.72	$2e_{1/2g}$	−10.74
			$3u_{3/2g}$	−10.71
$2t_{1u}$	88 F-2p; 7 U-6p; 5 U-5f	−10.22	$2e_{1/2u}$	−10.73
			$3u_{3/2u}$	−9.93
	Lowest Unoccupied			
$1a_{2u}$	100 U-5f	−7.08	$2e_{5/2u}$	−7.18
$2t_{2u}$	88 U-5f; 12 F-2p	−6.40	$4u_{3/2u}$	−6.36
			$3e_{5/2u}$	−6.26
$3t_{1u}$	88 U-5f; 12 F-2p	−5.11	$5u_{3/2u}$	−5.01
			$3e_{1/2u}$	−4.90
$2a_{1g}$	100 U-7s;	−0.77	$3e_{1/2g}$	−0.78
$2t_{2g}$	74 U-6d; 15 F-2p	−0.39	$4u_{3/2g}$	−0.56
			$2e_{5/2g}$	−0.11
$2e_g$	99 U-6d	+1.29	$5u_{3/2g}$	+1.29

[a] Labeled by irreps of the O_h group. [b] Labeled by irreps the O_h double group.

Spin−orbit coupling was treated with the state interaction RAS/SO approach.[43] The SO matrix elements between the scalar relativistic RAS CSFs were evaluated with the SOC operator of the RECP formalism. For the diagonal elements of the SO interaction matrix, the RASPT2 state energies were used. In ample cases[44] including uranyl,[34] such an approach provides an accuracy comparable to all-electron-based SOC calculations.[45]

The size of the SO matrix, coupling spin-singlet and spin-triplet CSFs, rises to 253 × 253 for the g-states, which becomes rather demanding. As a compromise we only included the lowest-lying 45 excited g-singlets and 45 g-triplets, together with the ground state, in the SO matrix for the g-states. So the dimension of the matrix was reduced to 181 × 181. Similarly for the u-states, the lowest 48 u-singlets and 48 u-triplets were chosen, resulting in a SO matrix of 192 × 192. Test calculations have shown that such a reduced RAS/SO scheme still gives a satisfactory accuracy.

All-electron relativistic TDDFT calculations, with or without SOC, were performed with the relativistic zeroth-order regular approximation (ZORA),[46,47] as implemented in the ADF 2008 program.[48−50] In the two-component scheme ZORA contains SOC terms of $(\sigma \cdot p\ \mathrm{V}\ \sigma \cdot p)$ type. We used STO basis sets of triple-ζ plus polarization (TZP) quality for U and of DZP quality for F, from the ADF basis sets library. The SAOP[51,52] and PW91[53] XC functionals were applied to compare the asymptote-corrected functional with common generalized gradient approximation (GGA) functional. For comparison, a parallel series of TDDFT calculations with RECP was carried out by employing the NWChem 5.1 program[54,55] with the same GTO basis sets and Stuttgart RECP as in the RAS calculations. In the NWChem calculations, we applied two pure density functionals (PW91 and BLYP)[56,57] and two hybrid ones (B3LYP[58] and BHLYP)[59] to examine the effects of different XC functionals.

RESULTS AND DISCUSSION

Electronic States. The ground state of UF_6 is known to be $^1A_{1g}$ with valence electron configuration $\cdots(1e_g)^4(1t_{2g})^6(1t_{1u})^6(1a_{1g})^2(1t_{2u})^6(1t_{1g})^6(2t_{1u})^6$ (Figure 1).[21] The DFT PW91 energies and AO compositions of the occupied and virtual MOs at the scalar and SO relativistic levels are listed in Table 2. The 18 highest occupied MOs around −13 to −10 eV are close in energy and consist of the 2p lone pairs of the F^- ligands with up to 20% of U-5f or U-6d and less U-6p or U-7s. The 7 lowest unoccupied MOs ($1a_{2u}$, $2t_{2u}$, and $3t_{1u}$) around −7 to −5 eV are dominantly U-5f with a highest occupied molecular orbital−lowest unoccupied molecular orbital (HOMO−LUMO) gap of 2.75 eV with SOC, which is small for a closed-shell molecule. The high-lying virtual MOs ($2a_{1g}$, $2t_{2g}$, and $2e_g$) of dominant U-7s and U-6d character are more than 4 eV above the U-5f ones because they are pushed up more than the contracted U-5f ones by the filled F-2p shells owing to their stronger overlap (Figure 1). The low-energy occupied MOs, more than 10 eV below the active occupied ones, are already of semicore U-6p and F-2s type. Thus, only single electron excitations of LMCT type from the F^--2p ligand shell to the U-5f shell occur in the region below 10 eV. The above-described RAS (2, 18, 2, 7) of 36 electrons and 18 + 7 orbitals with single and double excitations was thus chosen.

Spin−orbit coupling splits the triply degenerate t-type orbital levels of the ordinary O_h group into doubly and quadruply degenerate spinor levels of the double group: $t \otimes e_{1/2} = e_{1/2\ \mathrm{or}\ 5/2} \oplus u_{3/2}$. DFT calculations show that, as expected, the SO splitting of the occupied MOs of F-2p type remains small, in the range of 0.1 eV. The only exception is the $2t_{1u}$ HOMO with a SO splitting of ∼0.8 eV, due to the admixture[22] of 7% U-6p (Table 2) with a large atomic SOC effect of U-6p in the order of 11 eV. The $2t_{1u}$ excited states exhibit even larger SO splittings (see below) because the U-6p admixture of $2t_{1u}$ increases by about one-half upon one-electron depletion of the $2t_{1u}$ orbital. Thereby, SOC reduces the HOMO−LUMO gap, leading to comparatively small excitation energies for the lowest states of g-type.[22] Finally we have checked the flexibility of the basis sets by uncontracting the U-p functions,[60] and the energy changes of the SOC state energies were below 0.01 eV.

The double-group symmetries of the excited spin−orbit states are obtained in the usual manner. For instance, the first spin-averaged transitions $(2t_{1u} \rightarrow 1a_{2u})\ ^1A_{1g} \rightarrow {}^{3,1}T_{2g}$ generate a total of $(3 + 1) \times 3 = 12$ individual states, with two excitation energies of singlet−triplet and singlet−singlet types. Under SOC in the O_h^* double-group symmetry of a vibrationally undistorted UF_6 molecule, this splits up as follows (for more details, see Hay):[21]

$$u_{3/2u} \rightarrow e_{5/2u} : u_{3/2u} \otimes e_{5/2u} = E_g \oplus T_{1g} \oplus T_{2g}$$

$$e_{1/2u} \rightarrow e_{5/2u} : e_{1/2u} \otimes e_{5/2u} = A_{2g} \oplus T_{2g}$$

The calculated excitation energies of the g- and u-states at the SR- and SOC- RASPT2 levels up to nearly 10 eV are listed in the Supporting Information (Tables S1−S3). The excitation energies

Table 3. Theoretically Predicted Transition Energies (in eV) of Low-Lying Vertical Excited g-States of UF_6 in Comparison to Experimental Data

Scalar Relativistic Calculation				SOC Relativistic Calculation				Spectroscopic	
Orbital transition	El. state	This work [a]	Hay [b]	Spinor transition	El. state	Hay [b]	This work [a]	Solid UV Lewis [c]	El.Impact Cartwright [d]
$2t_{1u} \rightarrow 1a_{2u}$	$^3T_{2g}$	4.02	4.10	$(2t_{1u})3u_{3/2u} \rightarrow (1a_{2u})2e_{5/2u}$	$1T_{1g}$	3.35	3.33	3.046	3.22±0.01
	$^1T_{2g}$	4.27	4.55		$1E_g$	3.41	3.38		
					$1T_{2g}$	3.55	3.46	3.133	
$2t_{1u} \rightarrow 2t_{2u}$	$^3T_{2g}$	4.51	4.84						
	^3E_g	4.54	4.54		$2T_{2g}$	4.14	4.04	3.761	4.14±0.02
	$^1T_{1g}$	4.71	4.91		$2E_g$	4.12	4.10		
	$^3T_{1g}$	4.78	4.53	$(2t_{1u})3u_{3/2u} \rightarrow (2t_{2u})4u_{3/2u}$	$3T_{2g}$	4.39	4.14	3.848	
	$^1T_{2g}$	4.79	4.99		$2T_{1g}$	4.01	4.17		
	$^1A_{2g}$	4.87	5.12		$1A_{2g}$	4.36	4.25		
	$^3A_{2g}$	4.97	5.10		$3T_{1g}$	4.17	4.28	3.982	
	^1E_g	5.00	5.25		$1A_{1g}$	4.35	4.30		
$2t_{1u} \rightarrow 3t_{1u}$	^3E_g	5.50	5.41	$(2t_{1u})3u_{3/2u} \rightarrow (2t_{2u})3e_{5/2u}$	$4T_{2g}$	4.53	4.44	4.069	
	$^3A_{1g}$	5.57	5.52		$4T_{1g}$	4.43	4.47		
	$^3T_{1g}$	5.72	6.00		$3E_g$	4.56	4.53		
	$^1A_{1g}$	5.74	6.13						
	$^1T_{1g}$	5.88	6.13	$(2t_{1u})2e_{1/2u} \rightarrow (1a_{2u})2e_{5/2u}$	$2A_{2g}$	5.83	5.03		
	^1E_g	5.88	6.61		$5T_{2g}$	5.97	5.10		
	$^3T_{2g}$	5.92	6.08						
	$^1T_{2g}$	5.92	6.21		$5T_{1g}$	5.24	5.28		
					$6T_{2g}$	5.24	5.33		
					$6T_{1g}$	5.28	5.34		
				$(2t_{1u})3u_{3/2u} \rightarrow (3t_{1u})5u_{3/2u}$	$7T_{2g}$	5.59	5.38		
Etc.					$4E_g$	5.70	5.44		
					$2A_{1g}$	5.94	5.46		
					$3A_{2g}$	5.55	5.50		

[a] RASPT2, this work. [b] HF + 1, Hay.[21] [c] UV, solid phase, Lewis et al.[15] [d] Electron impact, gas phase, Cartwright et al.[16]

of all g-states up to about 5 eV and of the T_{1u} states up to about 10 eV are here displayed in Tables 3 and 4, respectively, together with Hay's (HF + 1) results[21] and the experimental data. Concerning the low-lying g-states, Hay's and our values (SR and SOC) agree within about 0.2 eV. However, for excited states above 5 eV, the discrepancy reaches 0.9 (0.7) eV for the SOC (SR) states of $2t_{1u} \rightarrow 3t_{1u}$ type, probably due to the limitation of electron correlation in Hay's CIS-like scheme. Accordingly, the rather dense energy-level order sometimes differs already for the low-lying states. Concerning the T_{1u} states, the agreement for the two lowest SR terms of $1t_{1g} \rightarrow 2t_{2u}$ and $1t_{1g} \rightarrow 3t_{1u}$ origin again is good (about 0.1 eV), while the discrepancies become larger for terms above 7 eV, where they reach 1.25 eV for $1e_g \rightarrow 3t_{1u}$. We attribute these enlarged discrepancies to the less reliable large-core pseudopotential used previously.[21]

Electronic Spectra. Experimental UV absorption spectra in condensed phase and electron-impact spectra in gas phase are known for UF_6 up to about 10 eV.[15,16,61] They involve mostly electric dipole allowed $A_{1g} \rightarrow T_{1u}$ transitions. Weaker transitions observable at energies below the onset of the strong ones may be magnetic dipole allowed ($A_{1g} \rightarrow T_{1\,g}$) or vibronically induced, in particular by the t_{1u} and t_{2u} bending vibrations, relevant for F-t_{1u} → U-5f excitations. Below 4.5 eV, 6 sharp UV absorption lines were observed in the solid (Table 3) and can be tentatively assigned to final $T_{1,2\,g}$ states, which occur 0.3 eV lower than calculated by RAS/SO. In the same energy range, two broader molecular electron-impact lines were observed. The corresponding groups of calculated transition energies lie at most about 0.1 eV higher. We note the large red shift of the solid-state spectra of about 0.2 eV, which is reminiscent of similarly large noble gas matrix effects for CUO and UO_2 molecules.[62−65]

The lowest g → g excitations near 3 eV originate from $(2t_{1u})$ $3u_{3/2u} \rightarrow (1a_{2u})$ $2e_{5/2u}$ orbital transitions. Compared to the SR energies, they are strongly spin−orbit stabilized by about 0.7 eV. The $(2t_{1u})$ $5e_{1/2u} \rightarrow (1a_{2u})$ $2e_{5/2u}$ spin−orbit mates are calculated

Table 4. Theoretically Predicted Excitation Energies (ΔE, in eV) and Transition Moments (μ, in Debye) of Low-Lying T_{1u} States of UF_6 in Comparison to Experimental Transition Energies

Orbital transition	Scalar Relativistic		Spin-Orbit Coupled		Spectroscopic
	This work [a]	Hay [b]	Hay [b]	This work [a]	El.Impact Cartwright [c]
$1t_{1g}\rightarrow 1a_{2u}$	-	-	5.39 (0.43)	4.98 (0.47)	4.77±0.18
$1t_{1g}\rightarrow 2t_{2u}$	5.95 (1.18)	6.10 (1.58)	6.01 (0.38)	5.63 (0.45)	5.41±0.06
			6.15	5.72 (0.13)	
			6.22 (0.69)	5.76 (0.98)	5.87±0.03
			6.40 (1.04)	6.00 (0.92)	
$1a_{1g}\rightarrow 2t_{2u}$	-	-	6.85 (0.67)	6.26 (0.70)	
$1t_{1g}\rightarrow 3t_{1u}$	6.87 (0.26)	6.82 (0.43)	7.05	6.82 (0.46)	6.60±0.03
			7.12 (0.51)	6.84 (0.33)	
			7.25 (0.46)	6.98 (0.79)	7.09±0.08
			7.63	7.17 (0.24)	
			7.65	7.19 (0.28)	
$1t_{2g}\rightarrow 1a_{2u}$	7.22 (0.05)	7.40 (0.30)	7.35 (0.30)	6.87 (0.45)	
			7.41 (0.23)	6.92 (0.08)	
$1a_{1g}\rightarrow 3t_{1u}$	7.60 (4.15)	8.35 (3.08)	7.90 (0.33)	7.50 (0.97)	
			8.75 (3.02)	7.86 (1.56)	7.92±0.04
$1t_{2g}\rightarrow 2t_{2u}$	7.74 (0.03)	7.97 (0.79)	8.06	7.67 (0.97)	
			8.10	7.73 (0.33)	
			8.23	7.84 (0.35)	
			8.36	7.88 (0.13)	
			8.38 (0.28)	7.90 (0.01)	
$1e_g\rightarrow 1a_{2u}$	-	-	7.96	7.07 (0.35)	
$1e_g\rightarrow 2t_{2u}$	7.81 (0.01)	8.63 (1.12)	8.48 (0.61)	7.64 (1.70)	
			8.70 (0.74)	7.97 (0.74)	
			8.99 (0.76)	8.06 (0.24)	
$1t_{2g}\rightarrow 3t_{1u}$	8.75 (0.35)	9.10 (0.58)	9.31		
			9.38 (0.51)		
			9.41		
			9.49 (0.48)		
$1e_g\rightarrow 3t_{1u}$	9.02 (7.66)	10.27 (4.65)	10.20		
			10.38 (0.48)		
			10.65 (4.45)		9.13±0.04

[a] RASPT2, this work. States above 8.5 eV were excluded from the SOC calculations. [b] HF + 1, Hay.[21] [c] Electron impact, experimental.[16]

1.7 eV higher and are no longer observable under the onset of the strongly allowed transitions. The SO splitting of 0.09 eV (701 cm^{-1}), assigned to $2t_{1u}$ in the UV matrix work,[15] seems too small by more than an order of magnitude. We interpret this small splitting as due to differential F-2p/U-5f Coulomb coupling restrained by U-6p SOC. The enlarged F-2p ($2t_{1u}$) SO splitting has already been discussed above and is also consistent with the photoelectron spectra (PES) of gaseous UF_6 (Figures 1 and 2 of ref 66). From there, a ($2t_{1u}$) $u_{3/2u} - e_{1/2u}$ SO-splitting of about 1.4−1.5 eV can be deduced. The second group of weak features near 4 eV emerges from ($2t_{1u}$) $3u_{3/2u} \rightarrow (2t_{2u})$ $4u_{3/2u}$, $3e_{5/2u}$. We attribute the comparatively large U-5f (t_{2u}) final-orbital SO-splitting of about 0.2 eV to the large effective positive charge of U in UF_6.

The calculated electric dipole-allowed T_{1u} excitation energies and transition moments are listed in Table 4 and are compared to

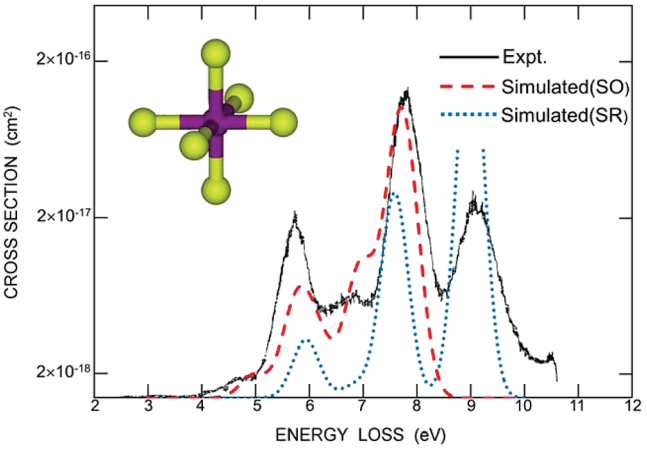

Figure 2. Experimental and theoretically simulated electric dipole-allowed electronic spectrum of UF_6. Solid curve: electron impact forward scattering;[16] dotted curve: SR calculation up to 9.5 eV; dashed curve: spin−orbit (SO) coupled calculation up to 8.5 eV.

the high-energy (75 eV) forward-scattering (5°) electron-impact features.[16] Our RASPT2/SO data reproduce the peak energies within about 0.2 eV. The lowest two T_{1u} states are calculated at 4.98 and 5.63 eV (corresponding to 5.39 and 6.01 eV from Hay's work)[21] with transition moments below 0.5 D and are hereby assigned as weak electric dipole-allowed spectral features. Concerning the experimental feature at 4.9 eV, our results show that it is not a forbidden transition, supporting the experimental assignment. The SOC wave function of the lowest T_{1u} state, for instance, is dominated by ($1t_{1g} \rightarrow 1a_{2u}$) $^3T_{2u}$; without SOC the transition would be singlet−triplet forbidden and 0.3 eV higher.

Figure 2 shows the comparison of the experimental electron-impact forward-scattering spectrum[16] and our SR- and SO-RASPT2 simulations. The 24 calculated T_{1u} transitions are represented by Gaussian functions with heights proportional to the squared transition moments and a full width at the half-maximum (fwhm) of 0.3 eV. The positions and relative intensities of the experimental features are reasonably reproduced by the SOC simulation. This gives credence to the validity of the slightly revised spectral assignments in Table 4. The simulation also explains why only 9 maxima were experimentally resolvable from the overlay of dozens of g → g and g → u transitions. While SOC shifts the peak positions of the SR curve only a little, it markedly changes the intensity pattern. The SR curve reproduces the position of the strong band near 9 eV but misses the weak peaks and shoulders below 5.5 eV. Our recent work also shows that applying this SO-RASPT2 approach, one can accurately predict the fluorescent states of UO_2F_2 and $UO_2F_2(Ar)x$ complexes.[67]

Dependence of RASPT2 Accuracy upon the RAS Level. As the accuracy of RASPT2 approaches depend on the type and number of allowed excitations in the RASSCF step, determined by the four parameters (n_1,M_1,n_3,M_3), we investigated various excitation levels (n_1,n_3). In as much as the (36,25) space is too large for performing comparable RASCF and CASSCF calculations, we carried out the test calculations with a (14,14) space. In such a size-reduced scheme, the number of CSFs in the CASSCF is 348 615, which is only 1/14000 of the CSFs number in CAS(36,25). For the 14 active orbitals, we selected the 7 upper occupied orbitals ($1a_{1g}$, $1t_{1g}$, and $2t_{1u}$) of nonbonding F-2p-type and the 7 low-lying empty orbitals ($1a_{2u}$, $2t_{2u}$, and $3t_{1u}$) of U-5f

Table 5. SR RASPT2 Excitation Energies (in meV) of UF_6

	Δ-RAS at level n[b]						
state[a]	n = 1	2	3	4	5	7	14 = CAS
1^1T_{2u}	−295.9	+38.0	+7.3	−0.2	+0.1	+0.0	4681.1
2^1T_{2u}	−251.1	+46.1	+8.8	−0.1	+0.2	+0.0	5304.7
1^1T_{1u}	−178.7	+41.6	+6.8	−0.2	+0.1	+0.0	5356.3

[a] For the three lowest electric dipole-allowed transitions to 1^1T_{2u}, 2^1T_{2u}, and 1^1T_{1u}. [b] Deviation at RAS levels (n,7,n,7) from the CAS(14,14) values (n = 14).

Table 6. NOON from SR MCSCF Calculations of UF_6 and UO_2^{2+} Ground States Using the R^2ASSCF Scheme

UF_6[a]	active NO	$1e_g$	$1t_{2g}$	$1t_{1u}$	$1t_{2u}$	$2t_{2u}$	$3t_{1u}$	$2t_{2g}$	$2e_g$
	occ. no.	1.988	1.991	1.992	1.981	0.020	0.006	0.009	0.012
UO_2^{2+}[b]	active NO	π_g	σ_g	π_u	σ_u	π_u^*	σ_u^*	π_g^*	σ_g^*
	occ. no.	1.973	1.973	1.962	1.976	0.039	0.038	0.026	0.013

[a] CAS(22,22)/RAS(2,11,2,11). [b] CAS(12,12)/RAS(2,6,2,6).

type. Choosing $M_1 = M_3 = 7$ and $M_2 = 0$ for the subspace partitioning, we varied $n_1 = n_3 = 1, 2, 3, ..., 14$, where for $n = 14$, the RAS reaches the complete active space (CAS).

For tests at the SR level, we investigated the 1^1A_{1g} ground state and three low-lying excited u-states (1^1T_{2u}, 2^1T_{2u}, and 1^1T_{1u}). The dependence of the excitation energies on parameter n is displayed in Table 5. Remarkably, the RASPT2 excitation energies quickly converge toward the CASPT2 results: For $n = 2$ (i.e., up to double excitations), the maximal absolute error is less than 0.05 eV, and it drops below 0.2 meV for $n \geq 4$. Since the computational cost increases dramatically with the excitation index, while the accuracy gain drops drastically, restriction to single and double excitations seems a good compromise for the present cases of LMCT transitions from ligand lone pairs to metal nonbonding orbitals of an otherwise closed-shell complex. The RASSCF approach with single and double excitations (hereafter denoted by R^2ASSCF) and additional RASPT2 calculations will be applied throughout this article, if not specified otherwise.

To obtain accurate results of the excitation energies, an important question is regarding how far occupied U-6p and virtual U-6d/7s orbitals are needed in the active space. Bonding and antibonding MOs involving U-6d and U-5f contribute considerably to correlation in the uranyl cation (UO_2^{2+}) and are usually included in the active space.[12,68] We have attempted to compare the U-6d contributions to the RASSCF results of UF_6 and UO_2^{2+} in their ground states with the R^2ASSCF scheme. For UF_6, an active space of (22,22) was constructed from the 11 occupied valence MOs that contain U-6d ($1e_g$, $1t_{2g}$) and U-5f ($1t_{1u}$, $1t_{2u}$) contributions, and their 11 unoccupied counterparts ($2t_{2u}$, $3t_{1u}$ and $2t_{2g}$, $2e_g$). The (12,12) active orbital set for UO_2^{2+} is formed by the 6 pairs of bonding/antibonding MOs, i.e., σ_u/σ_u^*, σ_g/σ_g^*, π_u/π_u^*, and π_g/π_g^*. The natural orbital occupation numbers (NOON) of the two molecular species are listed in Table 6.

As an approximate rule of thumb, for accurate multireference results natural orbitals with occupation number larger than 0.01 should be included in the CAS or RAS.[11,69,70] Table 6 shows that all 6 or at least 5 antibonding MOs of the triply bonded $[O{\equiv}U{\equiv}O]^{2+}$ should be included in the CAS as their NOONs exceed 0.025. The demand on the effective active space is less serious in the more ionically bonded U(-F)$_6$. With NO occupations around 0.01, the omission of U-6d type $2t_{2g}$ and $2e_g$ MOs from the active space should not lead to significant errors. Also the exclusion of U-6p orbitals from the RAS seems an acceptable compromise.

Table 7. SR Excitation Energies (in eV) for Low Singlets of UF_6 from SR-TDDFT Using Different Basis Sets and Various XC Functionals Compared to RASPT2 Results

	TDDFT						
	RECP[a]				all-electron ZORA[b]		
excited state	BLYP	PW91	B3LYP	BHLYP	PW91	SAOP	RASPT2 with RECP[a]
				g States			
1^1T_{2g}	3.16	3.17	3.83	4.81	3.27	3.88	4.27
1^1T_{1g}	3.73	3.73	4.21	5.00	3.82	4.54	4.71
2^1T_{2g}	3.79	3.80	4.25	5.02	3.91	4.62	4.79
1^1A_{2g}	3.74	3.74	4.26	5.19	3.82	4.54	4.87
1^1E_g	4.07	4.08	4.57	5.43	4.21	4.88	5.00
2^1T_{1g}	4.25	4.28	5.06	6.54	4.47	4.98	5.49
2^1A_{1g}	5.00	5.02	5.37	6.13	5.23	5.84	5.74
3^1T_{1g}	4.94	4.97	5.35	6.06	5.16	5.76	5.88
2^1E_g	4.98	5.01	5.57	6.35	5.22	5.81	5.88
3^1T_{2g}	4.93	4.95	5.45	6.11	5.15	5.77	5.92
ave dev[b]	−1.00	−0.98	−0.46	+0.41	−0.83	−0.21	
max dev[c]	−1.24	−1.21	−0.61	+1.05	−1.05	−0.51	
				u States			
1^1T_{2u}	3.45	3.44	4.38	5.97	3.63	4.25	5.24
1^1A_{2u}	4.19	4.18	4.93	6.33	4.40	5.09	5.69
1^1E_u	4.14	4.13	4.89	6.29	4.33	5.05	5.70
2^1A_{2u}	4.53	4.51	5.32	6.67	4.70	5.24	5.72
2^1T_{2u}	4.16	4.15	4.95	6.41	4.35	5.06	5.81
1^1T_{1u}	4.37	4.36	5.16	6.63	4.57	5.25	5.97
2^1T_{2u}	5.08	5.06	5.86	7.02	5.40	6.04	6.30
3^1T_{2u}	5.22	5.20	5.95	7.03	5.69	6.30	6.81
2^1T_{1u}	5.39	5.36	5.99	7.07	5.74	6.35	6.87
ave dev[c]	−1.51	−1.52	−0.74	+0.55	−1.24	−0.61	
max dev[d]	−1.79	−1.80	−0.88	+0.95	−1.61	−0.75	

[a] Same small-core potentials and basis sets as for RASPT2. [b] STO basis sets. [c] Average deviation from the RASPT2 results. [d] Maximal deviation from the RASPT2 results.

Evaluation of TDDFT. Even with simplifications by RASPT2 schemes, multiconfiguration WFT calculations are still expensive for actinide compounds, such as UF_6. It is thus worth investigating the quality of DFT and TDDFT approaches in the evaluation of the excited-state properties. Therefore, we have performed TDDFT calculations at the SR level using the all-electron ZORA and the valence-electron RECP approaches. The excitation energies for a number of low-lying excited singlets using different XC-functionals are shown in Table 7.

Obviously, the calculated excited states energies of UF_6 with TDDFT have significant errors when comparing to RASPT2 and experiments, at least concerning $(F\text{-}2p)_6 \rightarrow$ U-5f type excitations involving LMCT from extended orbitals to compact orbitals. All-electron ZORA and valence-electrons RECP results exhibit similar error patterns. For the PW91 functional, the two schemes do not differ by more than 0.2 eV. The two GGA functionals BLYP

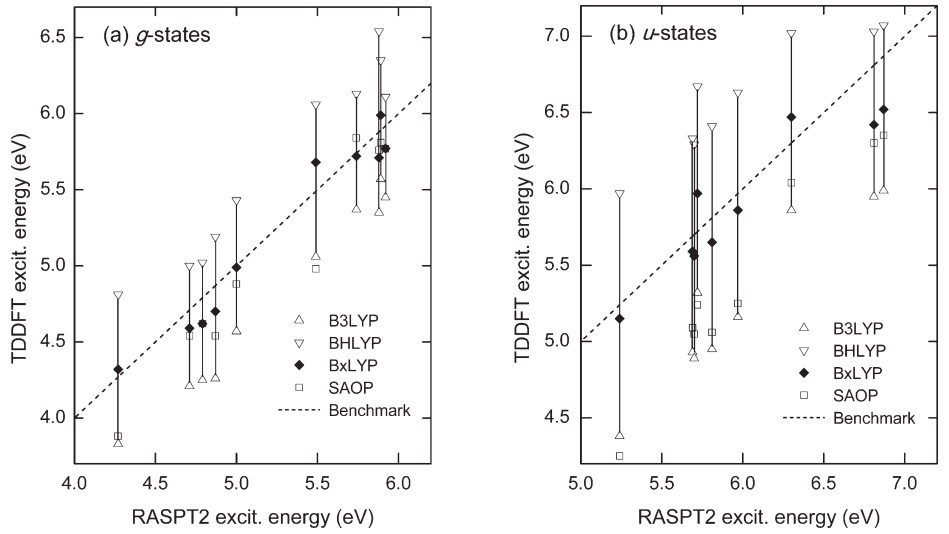

Figure 3. SR TDDFT excitation energies obtained by SAOP, B*x*LYP (with x = 35% HF exchange), B3LYP, and BHLYP.

and PW91 produce similar deviations, around −1 eV for the g-states and around −1.5 eV for the u-states. The two hybrid functionals B3LYP and BHLYP reduce the discrepancies to about one-half. Even the asymptotically corrected SOAP functional generates errors for the ungerade F-2p → U-5f type excitation energies of about −0.6 eV. Wahlgren et al. had speculated that the errors of TDDFT for the excited states may be due to the contributions from double excitations,[33] which are not accounted for by TDDFT. Among other error sources there is the incorrect asymptotic behavior of many XC functionals,[71] which leads to a typical underestimation of most excitation energies. This can be alleviated by XC functionals with adjusted asymptotic behavior like the SAOP. However, the SAOP functional still does not provide a satisfactory description of the LMCT states of UF_6.

The TDDFT energies of these charge-transfer transitions to very compact U-5f MOs seem particularly sensitive to the percentage of HF exchange in hybrid XC-potentials.[72] We note that adjusting the admixture of the HF exchange alleviates the DFT problems in the present case. As shown in Table 7, the HF exchange percentage increase from 20% (in B3LYP) to 50% (in BHLYP) turns the average deviation from −0.46 into +0.41 for the g-states and from −0.74 into +0.55 eV for the u-states. We therefore form a hybrid functional B*x*LYP with intermediate x = 35% HF exchange, which reproduces the RASPT2 excitation energies of UF_6 quite well (Figure 3). Further work is needed to investigate if this simple approach can help to predict the excited-states energies of other actinide compounds.

SUMMARY AND CONCLUSIONS

The electronic excited states involving transitions from F lone pairs to U-5f in UF_6 have been investigated by using an ab initio multireference electron correlation method. With the RASSCF-based approach, a single and double excitation restriction is shown to be acceptable for this type of transitions. With the Stuttgart small-core relativistic ECP and adapted one-electron basis sets, the spin−orbit interaction important for some of the transitions due to U-6p semicore admixture is accounted for by a RECP-SOC pseudopotential operator and the RASSCF/RASPT2/SO technique. Dynamic electron correlations are well recovered by second-order perturbation theory RASPT2. This scheme reproduces the spectral energies (within about 0.2 eV) and the intensities of the broad experimental electron-impact peaks below 10 eV. These transitions are of mixed singlet−triplet type. The two lowest-energy features are only vibronically and/or magnetic-dipole allowed, the next seven features are optically dipole allowed. Assuming a condensed phase red shift of 0.2 eV, the energies of the UV-absorption peaks in the optically forbidden region below 4.5 eV can also be well predicted. Given the numerous ligand lone pairs involved in the low-lying excited states, the quantitative prediction of the electronic spectra of UF_6 is computationally intensive. Our results represent so far the best theoretical reproduction of the few measured and the prediction of a large number of not yet detected excited states of UF_6. An improved tentative assignment of the measured excitations is given in Tables 3 and 4.

The presented RASSCF/RASPT2/SO technique using RECP appears as a promising tool for the investigation of the excited states of actinide compounds. It can serve as a benchmark for calibrating approximation approaches, such as SO-TDDFT, for applications in heavy-element systems. Even the asymptotically corrected SAOP functional is not yet sufficiently accurate for these comparatively simple one-electron excitations of actinide complexes. New exchange−correlation functionals that can handle charge-transfer and compact actinide 5f-states are needed for application of DFT and TDDFT for predicting the excited-states properties of actinide systems.

ASSOCIATED CONTENT

Supporting Information. Extended lists of excited-state energies are available free of charge via the Internet at http://pubs.acs.org/.

AUTHOR INFORMATION

Corresponding Author

*E-mail: junli@mail.tsinghua.edu.cn.

Present Addresses

†Permanent address: Physical and Theoretical Chemistry, Faculty of Science and Engineering, Siegen University, Siegen 57068, Germany. E-mail: schwarz@chemie.uni-siegen.de.

■ ACKNOWLEDGMENT

W.H.E.S. thanks for the hospitality of the Theoretical and Computational Chemistry Laboratory (TCCL). We acknowledge the financial support from NKBRSF (2011CB932400) and NSFC (20933003, 11079006, 91026003) of China. The calculations were performed using computers at the Supercomputing Center of the Computer Network Information Center, Chinese Academy of Sciences, Tsinghua National Laboratory for Information Science and Technology, and the Shanghai Supercomputing Center.

■ REFERENCES

(1) Hay, P. J.; Martin, R. L. *J. Chem. Phys.* **1998**, *109*, 3875–3881.
(2) Gagliardi, L.; Willetts, A.; Skylaris, C.-K.; Handy, N. C.; Spencer, S.; Ioannou, A. G.; Simper, A. M. *J. Am. Chem. Soc.* **1998**, *120*, 11727–11731.
(3) Xiao, H.; Li, J. *Chin. J. Struct. Chem.* **2008**, *27*, 967–974.
(4) (a) Hu, S.-W.; Wang, X.-Y.; Chu, W.-W.; Liu, X.-Q. *J. Phys. Chem. A* **2008**, *112*, 8877–8883. (b) Hu, S.-W.; Wang, X.-Y.; Chu, W.-W.; Liu, X.-Q. *J. Phys. Chem. A* **2009**, *113*, 9243–9248.
(5) Garrison, S. L.; Becnel, J. M. *J. Phys. Chem. A* **2008**, *112*, 5453–5457.
(6) De Jong, W. A.; Nieuwpoort, W. C. *Int. J. Quantum Chem.* **1996**, *58*, 203–216.
(7) García-Hernádez, M.; Lauterbach, C.; Krüger, S; Matveev, A.; Rösch, N. *J. Comput. Chem.* **2002**, *23*, 834–846.
(8) Larsson, S.; Tse, J. S. *Chem. Phys.* **1984**, *89*, 43–50.
(9) Andersson, K.; Malmqvist, P.-Å.; Roos, B. O.; Sadlej, A. J.; Wolinski, K. *J. Phys. Chem.* **1990**, *94*, 5483–5488.
(10) Andersson, K.; Malmqvist, P.-Å.; Roos, B. O. *J. Chem. Phys.* **1992**, *96*, 1218–1226.
(11) Pierloot, K. *Mol. Phys.* **2003**, *101*, 2083–2094.
(12) Pierloot, K.; Besien, E. *J. Chem. Phys.* **2005**, *123*, 204309.
(13) Küchle, W.; Dolg, M.; Stoll, H.; Preuss, H. *J. Chem. Phys.* **1994**, *100*, 7535–7542.
(14) Vallet, V.; Macak, P.; Wahlgren, U.; Grenthe, I. *Theor. Chem. Acc.* **2006**, *115*, 145–160.
(15) Lewis, W. B.; Asprey, L. B.; Jones, L. H.; McDowell, R. S.; Rabideau, S. W.; Zeltmann, A. H.; Paine, R. T. *J. Chem. Phys.* **1976**, *65*, 2707–2714.
(16) Cartwright, D. C.; Trajmar, S.; Chutjian, A.; Srivastava, S. *J. Chem. Phys.* **1983**, *79*, 5483–5493.
(17) Onoe, J.; Takeuchi, K.; Nakamatsu, H.; Mukoyama, T.; Sekine, R.; Adachi, H. *Chem. Phys. Lett.* **1992**, *196*, 636–640.
(18) Malli, G. L.; Styszynski, J. *J. Chem. Phys.* **1996**, *104*, 1012–1017.
(19) Hay, P. J.; Wadt, W. R.; Kahn, L. R.; Raffenetti, R. C.; Phillips, D. H. *J. Chem. Phys.* **1979**, *71*, 1767–1779.
(20) Evarestov, R. A.; Panin, A. I.; Bandura, A. V. *Russ. J. Gen. Chem.* **2008**, *78*, 1823–1835.
(21) Hay, P. J. *J. Chem. Phys.* **1983**, *79*, 5469–5482.
(22) Xiao, H.; Hu, H.-S.; Schwarz, W. H. E.; Li, J. *J. Phys. Chem. A* **2010**, *114*, 8837–8844.
(23) Malmqvist, P.-Å.; Pierloot, K.; Moughal Shahi, A. R.; Cramer, C. J.; Gagliardi, L. *J. Chem. Phys.* **2008**, *128*, 204109.
(24) Moughal Shahi, A. R.; Cramer, C. J.; Gagliardi, L. *Phys. Chem. Chem. Phys.* **2009**, *11*, 10964–10972.
(25) Sauri, V.; Serrano-Andrés, L.; Moughal Shahi, A. R.; Gagliardi, L.; Vancoillie, S.; Pierloot, K. *J. Chem. Theory Comput.* **2011**, *7*, 153–168.
(26) Gagliardi, L.; Heaven, M. C.; Krogh, J. W.; Roos, B. O. *J. Am. Chem. Soc.* **2005**, *127*, 86–91.
(27) Infante, I.; Andrews, L.; Wang, X.; Gagliardi, L. *Chem.—Eur. J.* **2010**, *16*, 12804–12807.
(28) (a) Berning, A.; Schweizer, M.; Werner, H.-J.; Knowles, P. J.; Palmieri, P. *Mol. Phys.* **2000**, *98*, 1823. (b) Figgen, D.; Müller, W.; Schweizer, M.; Stoll, H.; Peterson, K. A. *J. Chem. Phys.* **2003**, *118*, 4766–4767. (c) Peterson, K. A.; Shepler, B. C.; Singleton, J. M. *Mol. Phys.* **2007**, *105*, 1139–1155.
(29) Hafner, P.; Schwarz, W. H. E. *Chem. Phys. Lett.* **1979**, *65*, 537–541.
(30) Han, Y. K.; Hirao, K. *J. Chem. Phys.* **2000**, *113*, 7345–7350.
(31) Hay, P. J.; Martin, R. L. *J. Chem. Phys.* **1998**, *109*, 3875–3881.
(32) Peralta, J. E.; Batista, E. R.; Scuseria, G. E. *J. Chem. Theory Comput.* **2005**, *1*, 612–616.
(33) Réal, F.; Vallet, V.; Marian, C.; Wahlgren, U. *J. Chem. Phys.* **2007**, *127*, 214302.
(34) Wei, F.; Wu, G.-S.; Schwarz, W. H. E.; Li, J. *Theor. Chem. Acc.* **2011**, *129*, 467–481.
(35) Werner, H.-J.; Knowles, P. J.; Lindh, R.; Manby, F. R.; Schütz, M.; Celani, P.; Korona, T.; Mitrushenkov, A.; Rauhut, G.; Adler, T. B.; Amos, R. D.; Bernhardsson, A.; Berning, A.; Cooper, D. L.; Deegan, M. J. O.; Dobbyn, A. J.; Eckert, F.; Goll, E.; Hampel, C.; Hetzer, G.; Hrenar, T.; Knizia, G.; Koppl, C.; Liu, Y.; Lloyd, A. W.; Mata, R. A.; May, A. J.; McNicholas, S. J.; Meyer, W.; Mura, M. E.; Nicklass, A.; Palmieri, P.; Pflüger, K.; Pitzer, R.; Reiher, M.; Schumann, U.; Stoll, H.; Stone, A. J.; Tarroni, R.; Thorsteinsson, T.; Wang, M.; Wolf, A. *MOLPRO*, version 2008.1, a package of ab initio programs; University College Cardiff Consultants Limited: Wales, U.K., 2008; see http://www.molpro.net.
(36) Dunning, T. H. *J. Chem. Phys.* **1989**, *90*, 1007–1023.
(37) Seip, H. M. *Acta Chem. Scand.* **1965**, *20*, 2698–2710.
(38) Olsen, J.; Roos, B. O.; Jørgensen, P.; Jensen, H. J. A. *J. Chem. Phys.* **1988**, *89*, 2185–2192.
(39) Altmann, S. L.; Herzig, P. *Poing-Group Theory Tables*; Oxford University Press: Oxford, UK, 1994.
(40) Werner, H. J.; Meyer, W. *J. Chem. Phys.* **1981**, *74*, 5794–5801.
(41) Roos, B. O.; Andersson, K. *Chem. Phys. Lett.* **1995**, *245*, 215–223.
(42) Roos, B. O.; Andersson, K.; Fülscher, M. P.; Serrano-Andrés, L.; Pierloot, K.; Merchán, M.; Molina, V. *J. Mol. Struct. Theochem* **1998**, *388*, 257–276.
(43) Malmqvist, P. Å.; Roos, B. O.; Schimmelpfennig, B. *Chem. Phys. Lett.* **2002**, *357*, 230–240.
(44) Schimmelpfennig, B.; Maron, L.; Wahlgren, U.; Teichteil, C.; Fagerli, H.; Gropen, O. *Chem. Phys. Lett.* **1998**, *286*, 267–271.
(45) Ramírez-Solís, A.; Daudey, J. P. *J. Chem. Phys.* **2004**, *120*, 3221–3228.
(46) Chang, C.; Pelissier, M.; Durand, M. *Phys. Scri.* **1986**, *34*, 394–404.
(47) Faas, S.; Snijders, J. G.; van Lenthe, J. H.; van Lenthe, E.; Baerends, E. J. *Chem. Phys. Lett.* **1995**, *246*, 632–640.
(48) te Velde, G.; Bickelhaupt, F. M.; van Gisbergen, S. J. A.; Fonseca Guerra, C.; Baerends, E. J.; Snijders, J. G.; Ziegler, T. *J. Comput. Chem.* **2001**, *22*, 931–967.
(49) Fonseca Guerra, C.; Snijders, J. G.; te Velde, G.; Baerends, E. J. *Theor. Chem. Acc.* **1998**, *99*, 391–403.
(50) *ADF2009.01*, SCM, Theoretical Chemistry; Vrije Universiteit: Amsterdam, 2009; http://www.scm.com
(51) Gritsenko, O. V.; Schipper, P. R. T.; Baerends, E. J. *Chem. Phys. Lett.* **1999**, *302*, 199–207.
(52) Schipper, P. R. T.; Gritsenko, O. V.; van Gisbergen, S. J. A.; Baerends, E. J. *J. Chem. Phys.* **2000**, *112*, 1344–1352.
(53) Perdew, J. P.; Chevary, J. A.; Vosko, S. H.; Jackson, K. A.; Pederson, M. R.; Singh, D. J.; Fiolhais, C. *Phys. Rev. B* **1992**, *46*, 6671–6687.
(54) Straatsma, T. P.; Aprà, E.; Windus, T. L.; Bylaska, E. J.; de Jong, W.; Hirata, S.; Valiev, M.; Hackler, M.; Pollack, L.; Harrison, R.; Dupuis, M.; Smith, D. M. A.; Nieplocha, J.; Tipparaju, V.; Krishnan, M.; Auer, A. A.; Brown, E.; Cisneros, G.; Fann, G.; Früchtl, H.; Garza, J.; Hirao, K.; Kendall, R.; Nichols, J.; Tsemekhman, K.; Wolinski, K.; Anchell, J.; Bernholdt, D.; Borowski, P.; Clark, T.; Clerc, D.; Dachsel, H.; Deegan, M.; Dyall, K.; Elwood, D.; Glendening, E.; Gutowski, M.; Hess, A.; Jaffe, J.; Johnson, B.; Ju, J.; Kobayashi, R.; Kutteh, R.; Lin, Z.; Littlefield, R.; Long, X.; Meng, B.; Nakajima, T.; Niu, S.; Rosing, M.; Sandrone, G.; Stave, M.; Taylor, H.; Thomas, G.; van Lenthe, J.; Wong, A.; Zhang, Z. *NWChem, A Computational Chemistry Package for Parallel Computers*, version 5.1 (2006); Pacific Northwest National Laboratory: Richland, Washington , 2006.
(55) Kendall, R. A.; Aprà, E.; Bernholdt, D. E.; Bylaska, E. J.; Dupuis, M.; Fann, G. I.; Harrison, R. J.; Ju, J.; Nichols, J. A.; Nieplocha, J.;

Straatsma, T. P.; Windus, T. L.; Wong, A. T. *Comput. Phys. Commun.* **2000**, *128*, 260–283.
(56) Becke, A. D. *Phys. Rev. A* **1988**, *38*, 3098–3100.
(57) Lee, C; Yang, W.; Parr, R. G. *Phys. Rev. B* **1988**, *37*, 785–789.
(58) Becke, A. D. *J. Chem. Phys.* **1993**, *98*, 5648–5652.
(59) Becke, A. D. *J. Chem. Phys.* **1993**, *98*, 1372–1377.
(60) Weigend, F.; Baldes, A. *J. Chem. Phys.* **2010**, *133*, 174102 (10pp).
(61) (a) Bernstein, E. R.; Meredith, G. R. *Chem. Phys.* **1977**, *24*, 289-299, 301−309, 311−325. (b) Rice, W. W.; Oldenborg, R. C.; Wantuck, P. J.; Tiee, J. J.; Wampler, F. P. *J. Chem. Phys.* **1980**, *73*, 3560–3567. (c) Baranov, V. Y.; Kolesnikov, Y. A.; Kotov, A. A. *Quant. Electron.* **1999**, *29*, 653–666.
(62) Andrews, L.; Liang, B.; Li, J.; Bursten, B. E. *Angew. Chem., Int. Ed.* **2000**, *39*, 4565–4567.
(63) Li, J.; Bursten, B. E.; Liang, B.; Andrews, L. *Science* **2002**, *295*, 2242–2245.
(64) Li, J.; Bursten, B. E.; Liang, B.; Andrews, L. *J. Am. Chem. Soc.* **2002**, *124*, 9016–9017.
(65) Li, J.; Bursten, B. E.; Andrews, L.; Marsden, C. J. *J. Am. Chem. Soc.* **2004**, *126*, 3424–3425.
(66) Mårtensson, N.; Malmquist, P. Å.; Svensson, S.; Johansson, B. *J. Chem. Phys.* **1984**, *80*, 5458–5464.
(67) Su, J.; Wang, Y.-L.; Wei, F.; Schwarz, W. H. E.; Li, J. *J. Chem. Theory Comp.* **2011**; DOI: 10.1021/ct200419x.
(68) Gagliardi, L.; Roos, B. O. *J. Phys. Chem. A* **2001**, *105*, 10602–10606.
(69) (a) Pulay, P.; Hamilton, T. P. *J. Chem. Phys.* **1988**, *88*, 4926–4933. (b) Bofill, J. M.; Pulay, P. *J. Chem. Phys.* **1989**, *90*, 3637−3646; (c) Wolinski, K.; Pulay, P. *J. Chem. Phys.* **1989**, *90*, 3647–3659.
(70) Gordon, M. S.; Schmidt, M. W.; Chaban, G. M.; Glaesemann, K. R. *J. Chem. Phys.* **1999**, *110*, 4199–4207.
(71) Tozer, D. J.; Handy, N. C. *J. Chem. Phys.* **1998**, *109*, 10180–10189.
(72) Autschbach, J. *ChemPhysChem* **2009**, *10*, 1757–1760.